$V_{10}O_{28}^{6-}$, in which the decavanadate ion depolymerized to form oligomeric vanadate species at temperatures lower than 200 °C.[17] In the molybdate system, the lack of stable intermediates between the heptamolybdate and monomeric molybdates leads to the thermal stability of the ionic species. Drezdzon has also noted the stability of the heptamolybdate ion in magnesium aluminates based on thermal analysis data[12] but overestimated the stability to temperatures in excess of 500 °C. It is clear from the Raman spectrum showing in Figure 4f that samples heated to 450 °C result in reaction of the heptamolybdate ion with the magnesium aluminate framework. Raman bands at 347, 840, 860, 898, and 940 cm^{-1} characteristic of well-defined species are observed. On the basis of the reported Raman spectra of K_2MoO_4, $Na_2Mo_2O_7$, $(NH_4)_2Mo_2O_7$, and $MgMoO_4$,[29-32] these bands can be assigned to $MgMoO_4$ (940, 860, 840, 347 cm^{-1}) and $MgMo_2O_7$ (898 cm^{-1} $\nu_s(MoO_2)$), in agreement with the diffraction studies.

In conclusion, this study has shown two interesting aspects about the interlayer chemistry of molybdate ions in double metal hydroxides:

(a) The inability of MoO_4^{2-} to condense into oligomeric forms results in the destruction of the layer structure of $LiAl_2(OH)_6^+$ upon reaction of OH^- (hydrolyzed product of MoO_4^{2-}) with CO_2.

(b) $Mo_7O_{24}^{6-}$-intercalated $Mg_2Al(OH)_6^+$ can exist up to temperatures of 200 °C. At higher temperatures, the layer structure collapses, but the integrity of the $Mo_7O_{24}^{6-}$ is maintained until 400 °C.

Registry No. Al, 7429-90-5; LiCl, 7447-41-8; NaOH, 1310-73-2; $Mg(NO_3)_2$, 10377-60-3; $Al(NO_3)_3$, 13473-90-0; Na_2MoO_4, 7631-95-0; $LiAl_2(OH)_6Cl$, 68949-09-7; $LiAl_2(OH)_6 \cdot 1/2MoO_4$, 125615-48-7; $HMoO_4^-$, 14259-84-8; terephthalate-$Mg_2Al(OH)_6$, 117687-65-7; $Mg_2Al(OH)_6 \cdot 1/6Mo_7O_{24}$, 138721-91-2; $MgMoO_4$, 13767-03-8; $MgMo_2O_7$, 58478-77-6; terephthalic acid, 100-21-0.

(29) Issac, M.; Santha, N.; Nayar, V. U. *J. Raman Spectrosc.* **1991**, *22*, 237.
(30) Poloznikova, M. E.; Kondratov, O. I.; Fomichev, V. V. *Russ. J. Inorg. Chem.* **1988**, *33*, 348.
(31) Becher, H. J. *Z. Anorg. Allg. Chem.* **1981**, *474*, 63.
(32) Ozeki, T.; Murata, K.; Kihara, H.; Hikime, S. *Bull. Chem. Soc. Jpn.* **1987**, *60*, 3585.

Photoconductor Fatigue. 4. Effect of *p*-(Diethylamino)benzaldehyde Diphenylhydrazone Derivatives on the Photooxidation of the Charge-Transport Layer of Organic Layered Photoconductors

J. Pacansky,* R. J. Waltman, and R. Cox

IBM Almaden Research Center, 650 Harry Road, San Jose, California 95120-6099

Received September 27, 1991. Revised Manuscript Received January 9, 1992

The photooxidation of the hole-transport molecule *p*-(diethylamino)benzaldehyde diphenylhydrazone (DEH) gives rise to residual surface charges during light decay which cannot be photodischarged fast enough for electrophotographic applications. The "electrical fatigue" is attributed to a photochemically induced unimolecular rearrangement of DEH to an indazole derivative. By appropriate substitution of the DEH derivative, the photocyclization reaction and therefore the associated electrical fatigue in the corresponding organic photoconductor are eliminated. These results establish a clear relationship between photochemistry and electrical fatigue. Electrochemical and electrophotographic studies reveal that the hole-transport properties of the DEH derivatives remain the same as DEH despite the structural modifications. Additionally, an X-ray crystal structure analysis of a novel DEH derivative, OMDEH, is reported.

Introduction

The hole-transport molecule *p*-(diethylamino)benzaldehyde diphenylhydrazone (DEH) undergoes a photochemically induced unimolecular rearrangement to an indazole derivative, 1-phenyl-3-(4-(diethylamino)-1-phenyl)-1,3-indazole, with a quantum efficiency of 0.4.[1,2] Because hydrazones such as DEH are commonly used in hole transport in organic layered photoconductors, this photocyclization reaction to an indazole derivative has deleterious consequences on the electrical properties of the organic photoconductor. In particular, photoinduced discharge curves reveal the evolution of residual surface charges on the organic photoconductor during light decay which require decay times as long as several tens of minutes or more before the photoconductor is completely discharged.[3] Clearly, such photoconductors will fail in electrophotographic applications which require photodischarge in several tens of milliseconds. This degradation of the initial electrical properties of organic photoconductors is referred to as "electrical fatigue".

The requirements for high-volume printing capabilities (5×10^5 copies/month) on organic layered photoconductors put stringent requirements on their durability.[4] Thus electrical fatigue of organic photoconductors is important, and in recent studies[3,5,6] we have related changes in the

(1) Pacansky, J.; Coufal, H.; Waltman, R. J.; Cox, R.; Chen, H. *Radiat. Phys. Chem.* **1988**, *29*, 219.
(2) Pacansky, J.; Coufal, H.; Brown, D. W. *J. Photochem.* **1987**, *37*, 293.
(3) Pacansky, J.; Waltman, R. J.; Grygier, R.; Cox, R. *Chem. Mater.* **1990**, *3*, 454.
(4) Nakanishi, K. *Nikkei New Mater.* **1987**, 41.
(5) Pacansky, J.; Waltman, R. J.; Cox, R. *Chem. Mater.* **1990**, *3*, 903.

0897-4756/92/2804-0401$03.00/0

Scheme I

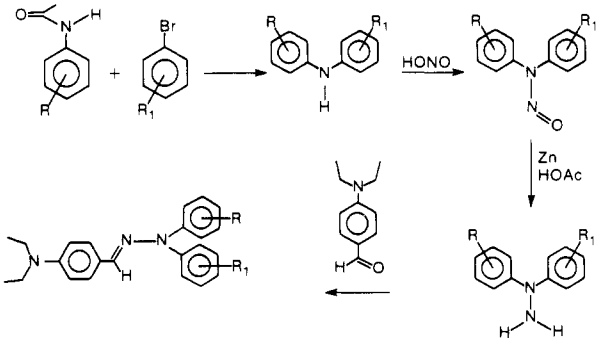

dark and light electrical properties to photochemistry initiated either at the interface between the charge-transport layer (CTL) and air or at the interface between the charge-generation (CGL) and charge-transport layers, respectively. In this paper, we pursue this matter further by investigating the effect of chemical substitution of DEH on its photochemical reaction and its subsequent effect on the electrical properties of organic photoconductors. The chemical modifications are aimed at suppressing the photocyclization reaction of DEH to the indazole derivative upon exposure to short-wavelength light. We observe that DEH photochemistry in the charge-transport layer and electrical fatigue are definitely correlated and furthermore may be significantly inhibited by suitable chemical substitution of the DEH moiety.

A thorough description of our model organic photoconductor is extant in the literature,[3] so no reiteration is necessary here. Briefly, the charge generation layer is composed of the bisazo pigment chlorodiane blue, and the charge-transport layer of 40% by weight of DEH (or DEH derivatives) in bisphenol A polycarbonate. These layers are formed sequentially atop an aluminum-coated polymer substrate to make up the layered organic photoconductor.

Experimental Section

Chlorodiane blue (CDB), polyester, and bisphenol A polycarbonate were obtained from commercial sources. Photoconductors were formulated in the following manner: coating sequentially, a 0.1-μm binder layer of polyester on aluminized polyethylene terephthalate was coated from tetrahydrofuran. The charge-generation layer was next coated, chlorodiane blue from ethylenediamine to a thickness of 0.1 μm. The charge-transport layer was next coated, 40% DEH in polymer(s) from tetrahydrofuran to a thickness of 20 μm. All layers were coated using the draw coating technique.

Synthesis of DEH Derivatives. The general synthetic procedure for the preparation of hydrazones is shown in Scheme I. An acetanilide is reacted with a bromobenzene to yield a diarylaniline which, in the presence of nitrous acid, is subsequently nitrosated to the *N*-nitroso product. Reduction with Zn yields the hydrazine which, in the presence of an aldehyde, yields the appropriate hydrazone. This general scheme was used to prepare DEH and all of its derivatives. The substituents R and R′ represent alkyl or aryl moieties. All of the chemical structures of DEH and its derivatives, and their acronyms, are summarized in Table I.

The following chemicals, obtained from commercial sources, were used directly: 4-(dimethylamino)benzaldehyde, 1,1-diphenylhydrazine hydrochloride, 4-methylacetanilide, *m*-toluidine, *p*-toluidine, 1-methyl-1-phenylhydrazine, and 2,6-dimethylaniline were obtained from Aldrich Chemical Co.; 2-methylacetanilide and *N*-phenyl-*N*-1-naphthylamine are from Eastman Organic Chemicals; 4-(diphenylamino)benzaldehyde is from Hodogaya Chemical Co.

(6) Pacansky, J.; Waltman, R. J. *Chem. Mater.* **1990**, *3*, 912.

Table I. Chemical Structures of DEH Derivatives[a]

acronym	colloquial name	R_1	R_2	R_3
DEH	DEH	CH_3CH_2—		H
OMDEH	*o*-methyl-DEH	CH_3CH_2—		H
DOMDEH	di-*o*-methyl-DEH	CH_3CH_2—		H
1NDEH	1-naphthyl-DEH	CH_3CH_2—		H
MMDEH	*m*-methyl-DEH	CH_3CH_2—		H
DPMDEH	di-*p*-methyl-DEH	CH_3CH_2—		—CH_3
DEH-DPA	DEH-diphenylamine			H
MPDEH-DEA	methylphenyl-DEH diethylamino	CH_3CH_2—	—CH_3	H
MPDEH-DPA	methylphenyl-DEH diphenylamino		—CH_3	H

[a] 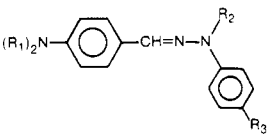

Table II. Properties of Hydrazones

compound	% yield	mp, °C	^{1}H NMR δ	IR (CH=N), cm^{-1}
OMDEH	33	110	1.2 t 6 H 2.7 s 3H 3.5 q 4H 6.6–7.5 m 14H	1594.6
DOMDEH	35	146	1.27 t 6H 2.1 s 6H 3.4 q 4H 6.7–7.6 m 13H	1599.3
1NDEH[a]	38	141	1.25 t 6H 3.4 q 4H 6.03–8.07 m 17H	1595.1
MMDEH	20	74	1.25 t 6H 2.3 s 3H 3.6 q 4H 6.8–7.9 m 14H	1603.3
DPMDEH	50	141	1.2 t 6H 2.4 s 6H 3.4 q 4H 6.5–7.9 m 13H	1598.6
MPDEH-DPA	65	93	3.4 s 3H 6.9–7.6 m 20H	1590.5
DEH	80	100	1.2 t 6H 3.3 q 4H 6.5–7.7 m 15H	1598
DEH-DPA	70	172	7.05–7.6	1589
MPDEH-DEA		157	3.4 s 3H 6.9–7.6 m 20H	1591

[a] German Patent DE 3331259 (*Chem. Abstr.* 101:31133).

General Preparation of Hydrazones. To a stirring solution of 20 mmol of an aldehyde in 50 mL of ethanol, 20 mmol of hydrazine was added in one portion, followed by 5–10 drops of concentrated HCl. Stirring at room temperature was continued for 2–3 h, after which the precipitate was filtered, washed with ethanol, and recrystallized. [If no precipitation occurs, the ethanol solution is evaporated and the residue poured into water and made slightly acidic. After extraction with ether, the aqueous acidic portion is separated, made slightly basic, and ether-extracted; the ether is washed with water and evaporated to give the hydrazone.] The product was identified by ^{1}H NMR and IR spectroscopies;

Table III. Properties of Diarylamines[a]

Y	X	Z	bp, °C	% yield	IR (N-H), cm^{-1}	^1H NMR ($CDCl_3$), δ
2-CH_3	H	H	135–40/0.8 mmHg	38	3390	2.3 s 3H 6.9–7.0 m 4H 7.2–7.3 m 5H
2-CH_3	H	6-CH_3	52[b]	80	3391	2.1 s 6H 6.3–7.3 m 8H
3-CH_3	H	H	130–40/0.1 mmHg	23	3391	2.4 s 3H 6.8–7.2 m 9H
4-CH_3	4-CH_3	H	135–39/0.2 mmHg	65	3407	2.3 s 6H 6.3 d 4H 7.2 d 4H

[a] 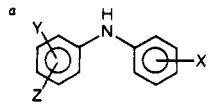 [b] Melting point.

Table IV. Properties of Nitrosoamines

X	Y	Z	% yield	IR (N–N=O) cm^{-1}	^1H NMR ($CDCl_3$), δ
2-CH_3	H	H	82	1446.2	1.99 s 3H 6.96 d 1H 7.2–7.5 m 8H
H	2-CH_3	6-CH_3	44	1446.0	2.03 s 6H 7.3–8.1 m 8H (CD_3COCD_3)
3-CH_3	H	H	48	1446.3	2.37 s 3H 6.86–7.5 m 9H
4-CH_3	H	4-CH_3	100	1446.0	2.4 s 6H 6.8–7.5 m 8H

[a] 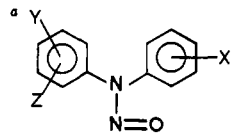

purity was established by thin-layer chromatography. Table II gives the yields, melting points, and spectral properties of the new hydrazones. Those for the parent DEH have already been published.[2]

Preparation of Diarylamines. The diarylamines were prepared by refluxing (up to 24 h) the appropriate acetanilide with a bromobenzene in the presence of anhydrous potassium carbonate and cuprous iodide.[7] Table III lists the yields, the boiling points, and the spectral properties for these secondary amines.

Preparation of Nitrosoamines. The nitrosoamines were prepared by reacting a solution of the secondary amine in ethanol at 5 °C, with a molar equivalent of an aqueous solution of sodium nitrite and excess concentrated HCl. After stirring for 0.5 h at room temperature, the reaction mixture was poured into water and ether-extracted. The extract was dried, the ether was removed, and the yellow oily nitroso compounds were used in the next step of the reaction (i.e., reduction to hydrazines) without further purification. Table IV summarizes the yields and spectral properties (^1H NMR and IR).

Preparation of Diarylhydrazines. The diarylhydrazones were prepared by the addition of zinc powder, added in several portions, to a solution of the nitrosoamine in an ethanol/acetic acid mixture. The addition was carried out at such a rate that the reaction temperature did not rise above 60 °C. Upon completion of the zinc addition, the reaction was stirred until a thin-layer chromatogram indicated that all the nitroso had reacted. The ethanol was evaporated, poured into water, and ether extracted. In all cases except for the 4,4-dimethyl and the 4-methyl derivatives, the reduction reaction gave a mixture of the secondary amine and a hydrazine. Although separation of the hydrazine could be accomplished by chromatography, the procedure was tedious; since the hydrazine content was readily estimated via ^1H NMR, the mixture was directly used in the subsequent reaction with the aldehyde to form the desired hydrazone.

Scheme II

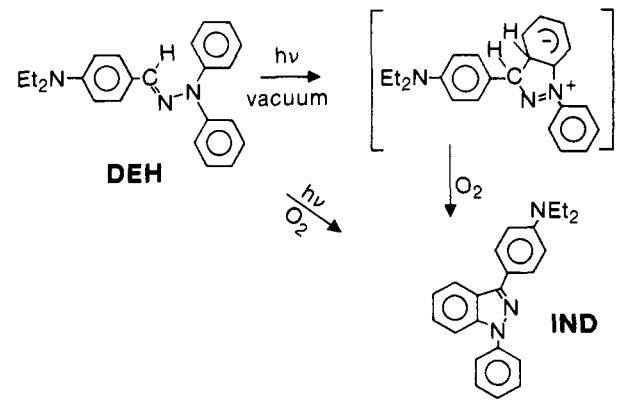

3-Methylacetanilide and 2,6-Dimethylacetanilide. These compounds were prepared by standard techniques[7] using acetic anhydride and a catalytic amount of sulfuric acid. The were isolated in 80–90% yields, and their spectral properties corresponded to literature values.

Electrical Fatigue Studies. For light fatigue studies of the electrical properties of the photoconductors, a fluorescent desk lamp (light source: Inter-World 8CW) with a spectral output ≃400–800 nm was used. The light emitted by the lamp was filtered with Corning CS 4-72 and 7-59 filters in tandem to allow transmission of light between 400 and 480 nm, termed "blue light". The incident energy on the sample surface was measured with a United Detector Technology Model 371 optical power meter equipped with a Model 262 head assembly; the blue light incident power was 0.22 mW/cm^2. The photoconductor samples were exposed to blue light in air at room temperature, then their electrical properties were measured by placing the photoconductors into a rotating disk electrometer, and their signal was analyzed.[8] The photoconductors in the rotating disk electrometer were discharged with long-wavelength light (520–750 nm) of incident energy 20 $\mu W/cm^2$.

For optical absorption studies of DEH photooxidation in the charge-transport layer (CTL), 0.3-μm CTL films were spin coated on optically flat quartz substrates and exposed to blue light. Exposures were carried out in air at room temperature using a Xe arc lamp filtered with 8 cm of water and CS 4-72 and 7-59 filters, respectively. The incident power was 11 mW/cm^2. UV–visible measurements were carried out using a Perkin-Elmer Lambda Array UV–visible spectrophotometer equipped with a Model 7700 computer.

Results and Discussion

As discussed in the Introduction, exposure of DEH in the charge-transport layer (CTL) to blue light (400–480 nm) gives rise to photocyclization of DEH to an indazole derivative (IND), as shown Scheme II. The indazole

(7) Freeman, H. S.; Butler, J. R.; Freeman, L. D. *J. Org. Chem.* **1987**, *43*, 4975.

(8) Pacansky, J.; Waltman, R. J.; Coufal, H.; Cox, R. *Radiat. Phys. Chem.* **1988**, *31*, 853.

derivative has been isolated and characterized by X-ray crystal structure, NMR, and standard spectroscopic techniques (UV–visible and infrared).[2] Associated with the photocyclization of DEH is electrical fatigue of the organic photoconductor; hence, it is our goal to structurally alter DEH to reduce the quantum yield for the photochemically induced rearrangement, while maintaining its original hole-transport properties.

The molecular structure of DEH consists of a planar π system from the aniline amine nitrogen atom to the diphenylhydrazone amine nitrogen atom, including one of the phenyl rings attached to the hydrazone amine at the other end of the molecule. The other phenyl group attached to the hydrazone amine is perpendicular to the π system.[2] Thus, both amine lone pairs lie in p orbitals that form the extended π system and hence are responsible for the basicity and low oxidation potential of the material and the characteristic low-energy chromophore (368 nm) in the optical absorption spectrum. Benzaldehyde diphenylhydrazone has an absorption band maximum at 342 nm, while dimethylaniline has one at $\simeq$300 nm. The lone pair of electrons on the hydrazone imine nitrogen are in an energetically low-lying sp^2 orbital and are of lesser importance.[9]

Since a mechanism for the ring closure from DEH to the indazole derivative IND involves rotation of one of the phenyl rings about the C–N bond to the hydrazone amine, a reasonable approach to retard the photocyclization is (1) to sterically hinder the torsional motion by replacing some of the phenyl hydrogens with alkyl groups like CH_3 or (2) to replace at least one of the phenyl rings with a saturated group that cannot cyclize in the first place. In addition, since the highest occupied molecular orbital of DEH consists for the most part of p–π orbitals housing the lone pairs of electrons on both the aniline and hydrazone amines, they must be involved in the electronic excitation that is responsible for the DEH photochemistry.[9] Consequently, the ethyl groups on the aniline nitrogens were also substituted by phenyl rings to determine the extent to which the aniline group may be involved in the photoprocess.

The DEH derivatives prepared for these studies are summarized in Table I. The DEH derivatives are characterized electrochemically first, to gain insight into the relative stability of the radical cations or "holes", and then formulated into organic photoconductors, and their photofatigue is investigated, both spectroscopically and electrically.

Electrochemical Characterization of DEH Derivatives. For a hole-transport molecule to be useful, it must have an appropriate ionization potential; a lower IP facilitates hole injection. Only DEH derivatives with suitable oxidation potentials and a low quantum yield for photodecomposition are acceptable. Because of this, we initially study preselected derivatives with suitable ionization potentials.

For simplicity, we may interpret the electrochemical oxidation potentials of DEH and its derivatives on a relative scale for their ionization potentials; this comparison is true only for molecules of similar structure and size since extrapolation to ionization potentials requires corrections for solvation energies:[10]

$$E_{1/2} = \mathrm{IP} - S^{ox} - c \qquad (1)$$

where $E_{1/2}$ is the half-wave oxidation potential, S^{ox} is the solvation energy, and c is an electrode constant. Thus, these data must be interpreted with caution due to the sensitivity of the parameter S. Nevertheless, cyclic voltammetry provides an excellent starting point for interpreting the effect of chemical derivatization of DEH on hole-transport properties because, as stated above, it provides a relative scale for hole injection efficiencies and it provides information on hole stabilities. The importance of the latter is that the redox reaction $DEH_1^{\bullet+} + DEH_2 \rightarrow DEH_1 + DEH_2^{\bullet+}$ may take place in the charge-transport layer (CTL) under an applied electric field before chemical restructuring may occur.

Table V. Electrochemical Data of DEH Analogues[a]

molecule	E_{pa}, V	$E_{pa/2}$ V	$\lvert E_{pa} - E_{pc}\rvert$, mV	i_{pa}/i_{pc}	n
DEH	0.58	0.52	60	1.0	1
OMDEH	0.57	0.51	65	1.0	1
DOMDEH	0.58	0.51	70	1.0	1
1NDEH	0.58	0.51	69	1.1	1
MMDEH	0.58	0.51	67	1.0	1
DPMDEH	0.54	0.47	70	1.0	1
MPDEH-DEA	0.53	0.46	70	1.1	1
MPDEH-DPA	0.74	0.67	75	1.2	1
DEH-DPA	0.80	0.73	70	1.1	1
MDEH	0.70	0.63	72	1.1	1

[a] Sweep rate = 60 mV/s.

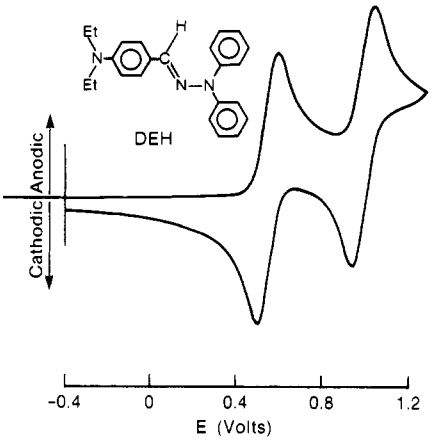

Figure 1. Cyclic voltammogram of DEH in 0.1 M tetraethylammonium fluoroborate/acetonitrile. Sweep rate = 60 mV/s.

Cyclic voltammetric data for DEH and its derivatives are summarized in Table V. The cyclic voltammetry of DEH, shown in Figure 1, reveals a reversible, two-wave redox reaction with peak oxidation potentials E_{pa} at 0.59 and 1.04 V. Consecutive scans just beyond the first E_{pa} reveal only a slight change in shape of the redox peak, attributed to a slight decrease of the concentration profile near the electrode surface until a diffusion-limited steady-state current is achieved. The cyclic voltammetry is characteristic of an electrooxidation reaction with no chemical reactions coupled to the charge transfer. The peak-to-peak separation $|E_{pa} - E_{pc}| = 60$ mV, and the ratio of the peak anodic to peak cathodic current $i_{pa}/i_{pc} = 1.0$. The n value was estimated from the Nicholson and Shain treatment[11] for a reversible electron transfer process; this is given in eq 2, where i_p is the peak current (mA), A is the

$$n = (i_p/272AD^{1/2}cv^{1/2})^{2/3} \qquad (2)$$

area of the working electrode (cm^2), D is the diffusion constant of the electroactive species (cm^2/s), c is the concentration (mmol/L) of the electroactive species, and v is the potential sweep rate (V/s). The diffusion constant

(9) Pacansky, J.; McLean, A. D.; Miller, M. D. *J. Phys. Chem.* **1990**, *94*, 90.

(10) Guttman, F.; Lyons, L. E. *Organic Semiconductors*; Wiley: New York, 1967; p 92.

(11) Nicholson, R. S.; Shain, I. *Anal. Chem.* **1964**, *36*, 706.

D for DEH in 0.1 M electrolyte/CH_3CN was estimated from the Stokes-Einstein equation:[12]

$$D = \frac{2.96 \times 10^{-7}}{\eta}\left(\frac{d}{M}\right)^{1/3} \quad (3)$$

where solution viscosity η = 0.00390 dyn s/cm^2 for 0.1 M electrolyte in CH_3CN, d = density in g/cm^3, and M = molecular weight. From the crystal structure of DEH,[2] d = 1.12 g/cm^3; and thus D_{DEH} = 1.1 × 10^{-5} cm^2/s and, correspondingly by using eq 2, n = 1. For the DEH derivatives, the density was assumed not to vary greatly from the parent molecule and thus d = 1.12 g/cm^3 was used in all cases; for example, the density of the DEH derivative OMDEH from crystal structure analysis was 1.12 g/cm^3. The n value was then calculated using eqs 2 and 3 and in all cases was unity. Thus, these data indicate that the redox reactions of DEH and its derivatives (Table V) are completely reversible with a simple electron transfer and no coupled chemical reactions. It is interesting to note that all of the peak oxidation potentials for the DEH derivatives are essentially the same, i.e., 570–580 mV, when R_1 = ethyl and R_2 and R_3 are phenyl or phenyl derivatives, as shown in Table V. We observe that the E_{pa} values change significantly when R_1 = phenyl, whereby the peak oxidation potentials increase by ≃200–250 mV (for DEH-DPA, MPDEH-DPA; see Tables I and V). This is readily explained in terms of a delocalization of the electron density on the aniline nitrogen atom into the R_1 phenyl rings and is well-documented for analogous systems.[12] We conclude from the electrochemistry of DEH and its derivatives that the hole-transport properties of the DEH derivatives are consistent with the parent DEH when R_1 = ethyl; hole injection efficiencies and hole stability are virtually identical. With these facts and the photorearrangement scheme in mind, several structural alterations to DEH to minimize photocyclization appear logical: (1) substitute the imine carbon hydrogen atom with some substituent such as methyl; or (2) sterically hinder the perpendicular phenyl ring attached to the hydrazone amine nitrogen atom. In this paper, we have focused on the latter, and the results are presented in the next section.

Photochemistry of DEH Derivatives. The optical absorption spectra as a function of blue light irradiation (400–480 nm) comparing the charge transport layers 40% DEH/polycarbonate, 40% OMDEH/polycarbonate, and 40% MPDEH-DEA/polycarbonate are shown in Figure 2 as illustrative examples. A normalized optical decay plot for all of the DEH derivatives (formulated to 40% by weight in a polymeric matrix) as a function of blue light is summarized in Figure 3. As we have observed previously,[3] DEH molecularly dispersed in polycarbonate and exposed to blue light in air photochemically converts to an indazole derivative. Thus the optical density of the 368-nm band maximum (Trace 1, Figure 2a) attributed to DEH, decreases as a function of incident energy, and there is a shift of the 368-nm band to shorter wavelengths. Concomitantly, a new band at 263 nm emerges attributed to the indazole derivative; an isosbestic point at 300 nm characterizes the photoconversion. After ≃30 J/cm^2 of blue light is incident on the organic photoconductor, most of the DEH has been converted to the indazole derivative.[3] Comparatively, the decay of the optical absorption spectrum of OMDEH in polycarbonate is significantly slower than the DEH/polycarbonate system (Figure 2b), a consequence of the *o*-methyl substituent on the perpendicular

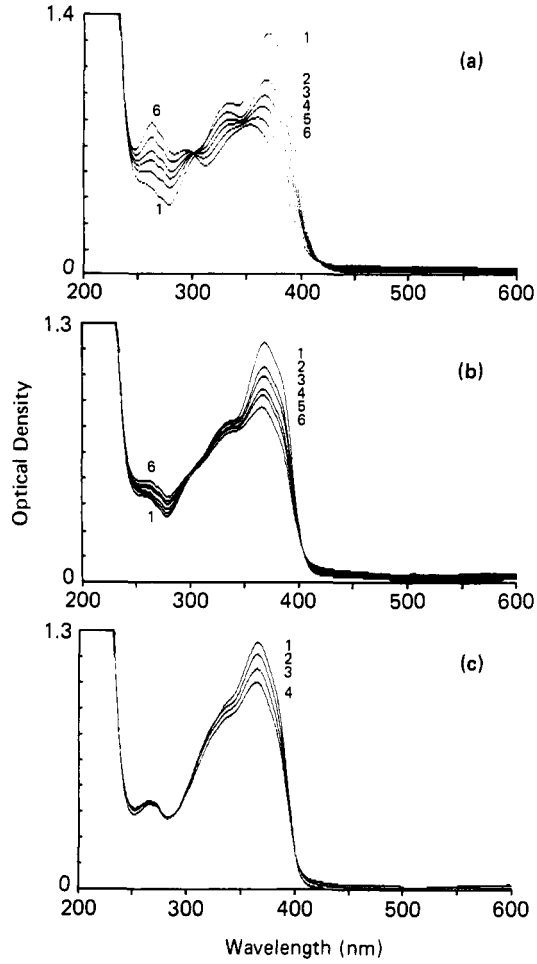

Figure 2. Optical absorption spectrum of (a) 40% by weight DEH in polycarbonate, (b) 40% OMDEH in polycarbonate, and (c) 40% MPDEH-DEA in polycarbonate as a function of incident blue light (10.9 mW/cm^2, λ 400–480 nm). For (a), traces 1–6 are 0, 3.3, 6.5, 9.8, 16.4, and 26.2 J/cm^2, respectively. For (b), traces 1–6 correspond to 0, 3.3, 21.6, 87, 126, and 211 J/cm^2, respectively. For (c), traces 1–4 equal 0, 8, 101, and 227 J/cm^2, respectively.

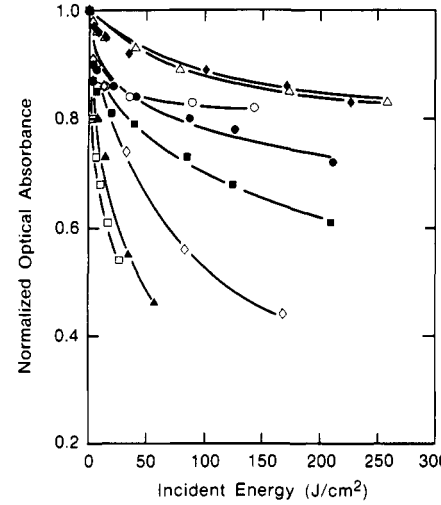

Figure 3. Summary plot of the normalized decay as a function of incident energy (blue light: 10.9 mW/cm^2, λ 400–480 nm) of the band maximum (≃370 nm) in the optical absorption spectrum of DEH derivatives, all 40% by weight in polycarbonate: DEH (□), MMDEH (▲), OMDEH (●), 1NDEH (■), DEH-DPA (◊), DOMDEH (○), MPDEH-DPA (△), and MPDEH-DPA (♦).

phenyl ring of the diphenylhydrazone moiety which retards the photocyclization reaction. Since one of two possible reaction sites on the phenyl is still available for photo-

(12) Nelson, R. F. In *Technique of Electroorganic Synthesis, Part 1*; Weinberg, N. L., Ed.; Wiley: New York, 1974; p 535.

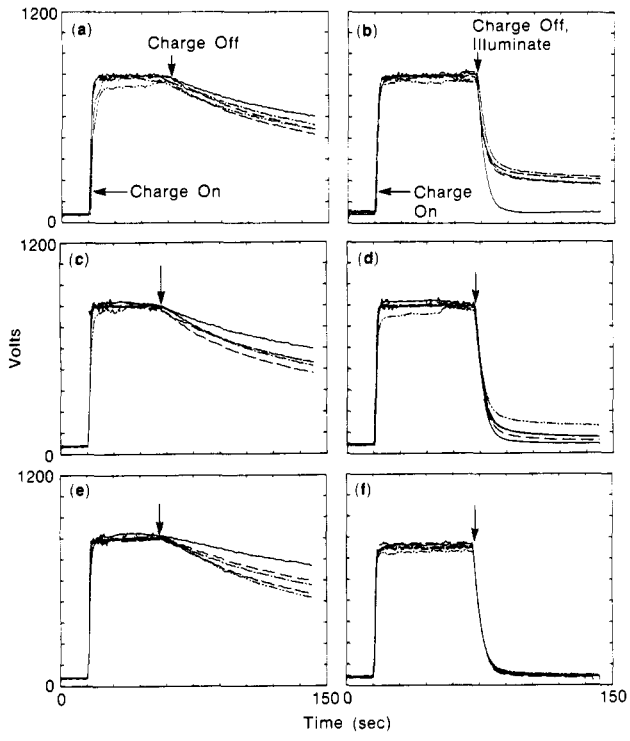

Figure 4. Dark and light decay curves for an organic photoconductor with a CTL derived from: (a) and (b) 40% by weight of DEH in polycarbonate; (c) and (d) 40% OMDEH in polycarbonate; and (e) and (f) 40% MPDEH-DEA in polycarbonate as a function of blue light exposure (0.22 mW/cm^2; 400–480 nm): 0 (—); 0.8 (– – –); 2.4 (– · –); 4.0 (– · · –); and 15.8 J/cm^2 (– – –).

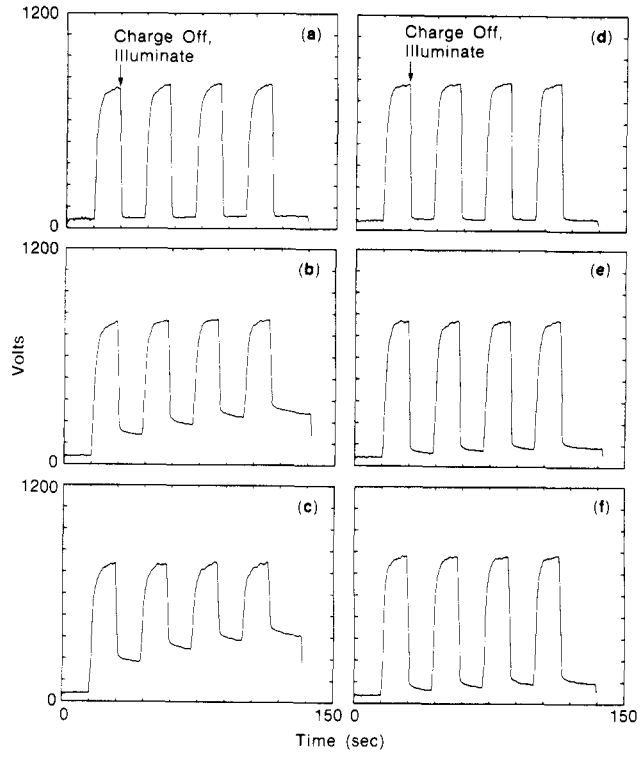

Figure 5. Photoinduced discharge (PID) curves as a function of incident blue light (0.22 mW/cm^2, λ 400–480 nm) showing four consecutive charge/photodischarge cycles. The PID curves are recorded after the photoconductor samples are exposed to blue light. Photodischarge is achieved by exposure of the photoconductors with yellow light (12 mW/cm^2, λ 500–800 nm). Parts a–c are for a photoconductor with a CTL derived from 40% DEH–DPA in polycarbonate, and parts d–f are for 40% MPDEH–DPA in polycarbonate. The blue light incident on the samples are (a) and (d) 0, (b) and (e) 0.8, (c) and (f) 18 J/cm^2.

cyclization, we observe formation of an indazole derivative with a characteristic absorption at 263 nm similar to IND but clearly at a significantly reduced rate. When the perpendicular phenyl ring bonded to the hydrazone amine nitrogen atom is replaced by methyl, the photocyclization reaction appears to be eliminated (Figure 2c) as shown by the absence of the 263-nm band even after several hundred J/cm^2 of incident energy. In this case, the phenyl substituent is no longer available for photocyclization; another channel for photochemistry is opened, but fortunately with a much lower efficiency. The summary plot shown in Figure 3 basically reiterates the experimental findings discussed above. Methyl substitution at the meta or para positions of the phenyl ring have no effect on inhibiting the photocyclization (see for example, MMDEH) while DOMDEH, wherein both ortho positions of the perpendicular phenyl ring are substituted by a methyl, approaches the behavior of MPDEH–DEA or MPDEH–DPA. Substitution of the alkyl groups on the aniline nitrogen by phenyl rings has no apparent effect on the photocyclization reaction at the hydrazone end of the system.

Changes in Electrical Properties. The dark and light decay curves as a function of incident blue light (400–480 nm) for a photoconductor formulation composed of a CTL of 40% by weight of DEH in polycarbonate (PC), 40% OMDEH/PC, and 40% MPDEH–DEA/PC are shown in Figure 4 as illustrative examples. As shown in Figure 4a, the major effect of incident blue light on a DEH-based organic photoconductor is the evolution of residual surface potential during light decay. Less than 1 J/cm^2 of incident blue light is sufficient to cause a significant rise in residual voltage, ≃130 V above ambient values. Comparatively, the rise in residual voltage is only ≃50 V for an OMDEH-based photoconductor (Figure 4b), and no excess residual voltage is observed at all for a MPDEH–DEA-derived photoconductor (Figure 4c), under these conditions. These results exactly parallel the photochemical results discussed above and provide strong evidence that the photochemical rearrangement to an indazole derivative is indeed associated with the increase in residual surface potential during light decay. More importantly, we have demonstrated that by appropriate substitution of the DEH molecule, in particular at the perpendicular phenyl ring of the diphenylhydrazone moiety, the photochemistry may be controlled to the point where it is rendered innocuous.

The origin for the residual surface potential and its relationship to the photochemistry has been discussed in detail elsewhere,[3,13] so no reiteration is necessary here. Figure 5 illustrates the evolution of the residual surface potential more vividly; here we compare DEH–DPA where the photocyclization is uninhibited with MPDEH–DPA where the perpendicular phenyl ring at the hydrazone end is replaced with a methyl. By consecutively charging and discharging (with light) the two photoconductors, we observe the rapid evolution of residual voltage with DEH–DPA but not with MPDEH–DPA. A summary plot for the evolution of residual voltage as a function of exposure to incident blue light for all of the DEH derivatives tested is shown in Figure 6. The curves appear to break into three regions: photoconductors formulated from DEH derivatives with the unsubstituted phenyl ring give rise to the highest residual voltages, ≃350 V after 2 J/cm^2. Those with a methyl substituent at an ortho position give rise to ≃200 V after 2 J/cm^2. When the phenyl is replaced with a methyl, there is little residual surface potential after

(13) Waltman, R. J.; Pacansky, J.; Bates, C. W., manuscript in preparation.

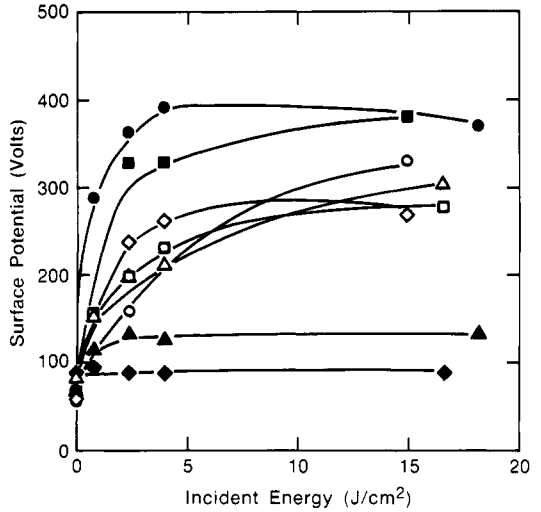

Figure 6. Residual surface potential on photoconductor after exposure to blue light (0.22 mW/cm^2; λ = 400–480 nm) and subsequent photodischarge (light decay). The charge transport molecules are 40% by weight in polycarbonate: DEH (■); DEH–DPA (●); 1NDEH (○); OMDEH (◇); MMDEH (△); DOMDEH (□); MPDEH–DPA (▲); and MPDEH–DEA (♦).

Scheme III

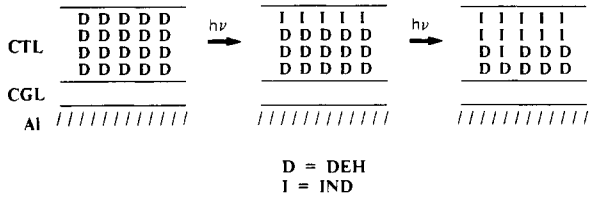

2 J/cm^2. The origin of the residual surface charges is attributed to the formation of a heterogeneous charge-transport layer containing an interface of DEH and the indazole derivative, as shown in Scheme III. In this model, hole transport under an externally applied electric field requires hole injection from DEH into the indazole derivative IND, before the negative surface charges can be annihilated. IND, having a much higher ionization potential than DEH, causes the holes to be trapped on DEH at the DEH/IND interface; consequently, the holes never reach the surface of the organic photoconductor and thus a residual surface potential develops. The residual charges after light decay is explained using an energy level model for the DEH/IND heterojunction, whereby the energy barrier for hole injection from DEH to IND is investigated as a function of applied field.[13] These studies conclude that the energy barrier could be overcome at high fields (e.g., 900 V/20 μm), but at lower fields, enough energy could not be extracted from the external field for the holes (i.e., DEH$^{\bullet+}$) to be injected into IND; consequently, at low fields, the holes become trapped in the CTL and do not reach the negatively charged photoconductor surface.

Crystal Structure of OMDEH. Due to the enhanced resistance to photochemistry and electrical fatigue of OMDEH to short-wavelength light and coupled with its excellent coating processability in bisphenol A polycarbonate, further characterization of the novel DEH derivative OMDEH was warranted, and the X-ray crystal structure is reported herein. Crystals of OMDEH are readily prepared from tetrahydrofuran yielding rather colorless, plate-shaped crystals.

The X-ray crystal structure analysis was performed by the Molecular Structure Corporation, College Station, TX. The OMDEH crystal structure was solved by direct methods. Hydrogen atoms were included in the structure

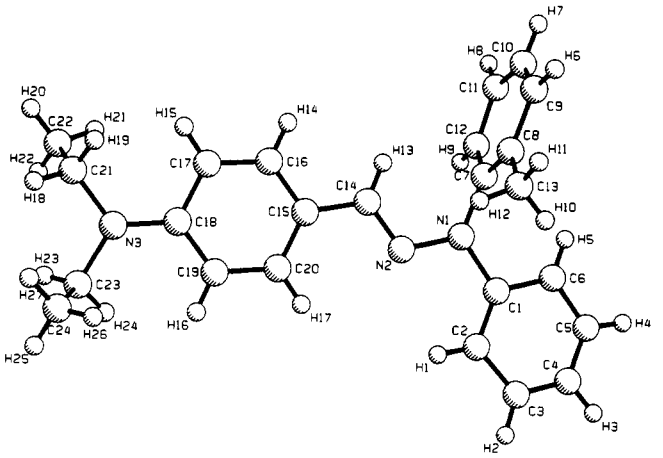

Figure 7. X-ray crystal structure of OMDEH.

Table VI. Crystal Data for OMDEH

empirical formula	$C_{24}H_{27}N_3$
formula weight	357.50
crystal color, Habit	colorless, plate
crystal system	monoclinic
space group	$P2_1$
lattice parameters	a = 7.388 Å
	b = 7.766 Å
	c = 18.685 Å
	β = 96.81°
Z value	2
d, g/cm^3	1.12
F_{000}	384
μ, cm^{-1}	0.62
no. of reflections	2200 total; 2035 unique (R_{int} = 0.050)
structure solution	direct methods
refinement	full-matrix least-squares
function minimized	$\sigma w(\|F_o\| - \|F_c\|)^2$
least-squares weights	$4F_o^2/\sigma^2(F_o^2)$
no. of observations $F_o^2 > 3\sigma(F_o^2)$	574
no. of variables	108
residuals	R = 0.086, R_w = 0.085
goodness of fit	2.60

Table VII. Crystal Bond Lengths (Å) for OMDEH. All C–H Bonds Set to 0.95

atom 1	atom 2	length	atom 1	atom 2	length
N1	N2	1.42	C8	C13	1.36
N1	C7	1.45	C8	C9	1.43
N1	C1	1.49	C9	C10	1.34
N2	C14	1.31	C10	C11	1.30
N3	C18	1.40	C11	C12	1.38
N3	C21	1.47	C14	C15	1.44
N3	C23	1.53	C15	C20	1.38
C1	C2	1.35	C15	C16	1.38
C1	C6	1.45	C16	C17	1.38
C2	C3	1.43	C17	C18	1.43
C3	C4	1.33	C18	C19	1.37
C4	C5	1.31	C19	C20	1.40
C5	C6	1.40	C21	C22	1.48
C7	C8	1.36	C23	C24	1.35
C7	C12	1.37			

factor calculation with ideal C–H bond lengths of 0.95 Å. The crystal structure of OMDEH is shown in Figure 7. Table VI contains the pertinent crystal data for OMDEH. The crystal system for OMDEH is monoclinic with 2 molecules/unit cell and crystallizes in the space group $P2_1$. The overall important features of the OMDEH crystal structure are that there is an extended π system from the amine nitrogen atom of the diethylaniline portion of the molecule to a phenyl group of the diphenylhydrazone moiety, and that the other phenyl ring attached to the diphenylhydrazone group, i.e., the tolyl group, is nearly

Table VIII. Crystal Bond Angles (deg) for OMDEH

atom 1	atom 2	atom 3	angle	atom 1	atom 2	atom 3	angle
N2	N1	C7	122	C13	C8	C9	117
N2	N1	C1	112	C7	C8	C9	123
C7	N1	C1	125	C10	C9	C8	110
C14	N2	N1	115	C11	C10	C9	128
C18	N3	C21	122	C10	C11	C12	123
C18	N3	C23	121	C7	C12	C11	114
C21	N3	C23	115	N2	C14	C15	117
C2	C1	C6	124	C20	C15	C16	118
C2	C1	N1	123	C20	C15	C14	126
C6	C1	N1	112	C16	C15	C14	116
C1	C2	C3	116	C15	C16	C17	123
C4	C3	C2	119	C16	C17	C18	120
C5	C4	C3	125	C19	C18	N3	123
C4	C5	C6	122	C19	C18	C17	117
C5	C6	C1	114	N3	C18	C17	121
C8	C7	C12	122	C18	C19	C20	123
C8	C7	N1	119	C15	C20	C19	120
C12	C7	N1	119	N3	C21	C22	114
C13	C8	C7	119	C24	C23	N3	104
H1	C2	C1	122	H14	C16	C15	119
H1	C2	C3	122	H14	C16	C17	119
H2	C3	C4	120	H15	C17	C16	120
H2	C3	C2	120	H15	C17	C18	120
H3	C4	C5	118	H16	C19	C18	119
H3	C4	C3	118	H16	C19	C20	119
H4	C5	C4	119	H17	C20	C15	120
H4	C5	C6	119	H17	C20	C19	120
H5	C6	C5	123	H19	C21	H18	109
H5	C6	C1	123	H19	C21	N3	108
H6	C9	C10	125	H19	C21	C22	108
H6	C9	C8	125	H18	C21	N3	108
H7	C10	C11	116	H18	C21	C22	108
H7	C10	C9	116	H20	C22	H21	109
H8	C11	C10	118	H20	C22	H22	109
H8	C11	C12	119	H20	C22	C21	109
H9	C12	C7	123	H21	C22	H22	109
H9	C12	C11	123	H21	C22	C21	109
H11	C13	H10	109	H22	C22	C21	109
H11	C13	H12	109	H23	C23	H24	109
H11	C13	C8	109	H23	C23	C24	111
H10	C13	H12	109	H23	C23	N3	111
H10	C13	C8	109	H24	C23	C24	111
H12	C13	C8	109	H24	C23	N3	111
H13	C14	N2	121	H26	C24	H27	110
H13	C14	C15	121	H26	C24	H25	109
H26	C24	C23	109	H27	C24	C23	109
H27	C24	H25	109	H25	C24	C23	109

Table IX. Crystal Dihedral Angles (deg) for OMDEH

atom 1	atom 2	atom 3	atom 4	angle	atom 1	atom 2	atom 3	atom 4	angle
N1	N2	C14	C15	180	C7	C8	C9	C10	2
N1	C7	C8	C13	5	C7	C12	C11	C10	5
N1	C7	C8	C9	-178	C7	N1	N2	C14	5
N1	C7	C12	C11	175	C8	C7	C12	C11	-1
N1	C1	C2	C3	180	C8	C9	C10	C11	2
N1	C1	C6	C5	-179	C9	C10	C11	C12	-6
N2	C14	C15	C20	2	C9	C8	C7	C12	-2
N2	C14	C15	C16	-177	C10	C9	C8	C13	178
N2	N1	C7	C8	88	C12	C7	C8	C13	-179
N2	N1	C7	C12	-88	C14	C15	C20	C19	-179
N2	N1	C1	C2	-6	C14	C15	C16	C17	-179
N2	N1	C1	C6	170	C15	C20	C19	C18	-1
N3	C18	C19	C20	180	C15	C16	C17	C18	-3
N3	C18	C17	C16	-178	C16	C15	C20	C19	0
C1	C2	C3	C4	-3	C16	C17	C18	C19	2
C1	C6	C5	C4	-1	C17	C16	C15	C20	2
C1	N1	N2	C14	180	C17	C18	C19	C20	0
C1	N1	C7	C8	-86	C17	C18	N3	C21	-2
C1	N1	C7	C12	97	C17	C18	N3	C23	159
C2	C1	C6	C5	-2	C18	N3	C21	C22	82
C2	C1	N1	C7	169	C18	N3	C23	C24	112
C2	C3	C4	C5	0	C19	C18	N3	C21	178
C3	C4	C5	C6	2	C19	C18	N3	C23	-20
C3	C2	C1	C6	4	C21	N3	C23	C24	-85
C6	C1	N1	C7	-15	C22	C21	N3	C23	-81

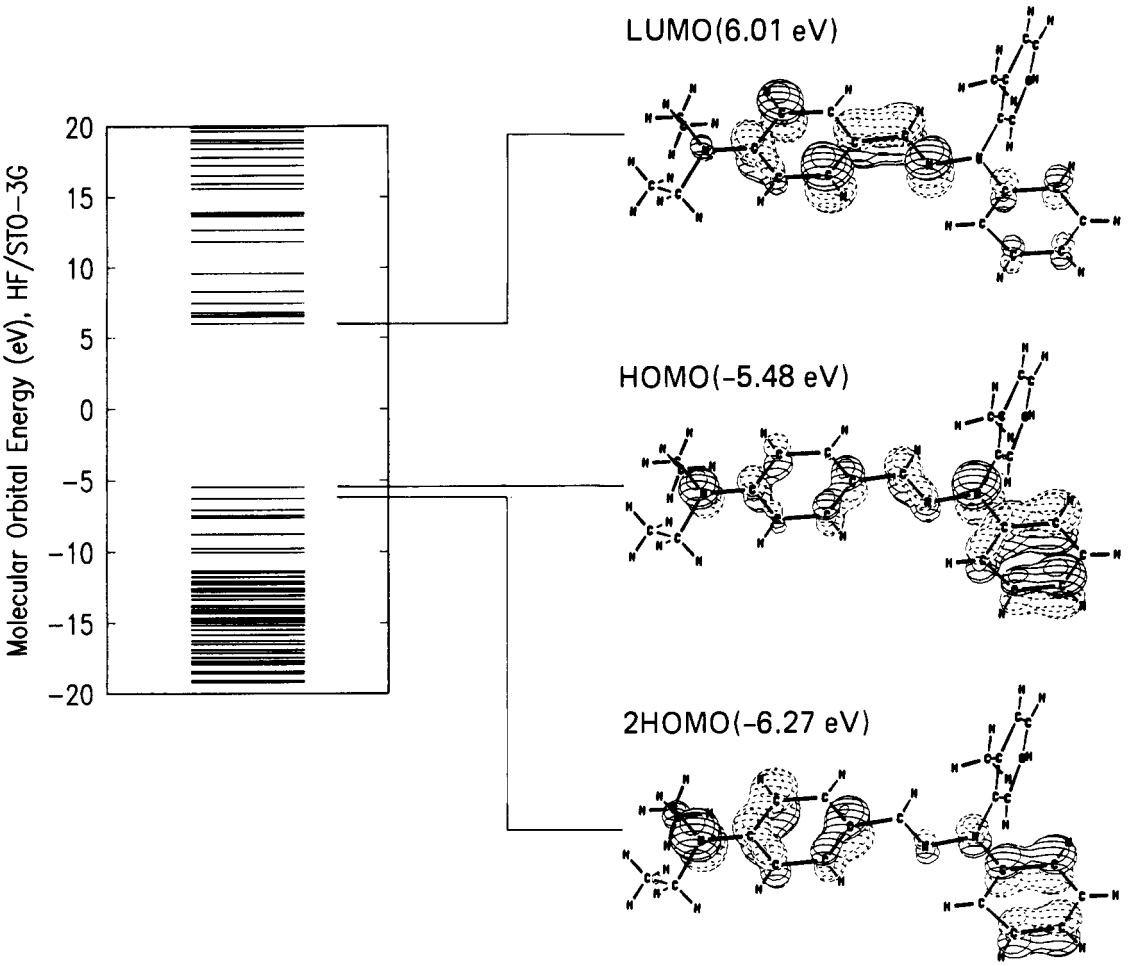

Figure 8. RHF/STO-3G molecular orbital pictures for the HOMO and 2HOMO of OMDEH at the crystal geometry. The total energy was -1073.676 161 5 hartrees.

perpendicular, being twisted by 86° relative to the extended π plane. Thus the overall molecular structure resembles its parent DEH in every aspect.[2] WIth respect to photochemistry and electrical fatigue of OMDEH, however, the most important result here is that it is the tolyl group that is perpendicular to the molecular π plane. In view of the photocyclization reaction presented above, we conclude that the methyl substituent does indeed inhibit the photocyclization of DEH to the indazole derivative since it is the perpendicular phenyl ring that is involved in the photocyclization. Because the tolyl structure on the hydrazone end inhibits the photochemistry, this accounts for the improved electrical properties of the OMDEH-derived organic photoconductor. Finally, unlike the case for the parent DEH,[2] there is apparently only a trans configuration of the ethyl groups in the diethylaniline portion of the molecule. The crystal structure and pertinent bond lengths, angles, and torsions are summarized in Figure 7 and Tables VII–IX.

As with the parent hydrazone DEH, OMDEH forms an extended π system from the amine nitrogen atom N3 to, and including, the almost coplanar phenyl ring at the other end of the molecule. This certainly means that the lone pair of electrons on the nitrogens N3 and N1 (see Figure 7) are delocalized into the π system. An orbital picture[14,15] for the highest occupied molecular orbital (HOMO) is shown in Figure 8. The OMDEH HOMO is a direct manifestation of the delocalized π system which extends from the aniline amino group to the coplanar phenyl ring at the opposite end of the molecule. The perpendicular tolyl group bonded to the hydrazone amine contributes negligibly to the HOMO. The second highest occupied molecular orbital, or 2HOMO, is also a reflection of the extended π system. The effect of this delocalization is to lower the energy required for ionization, for example, electrooxidation, and thus this series of molecules all have low electrochemical oxidation potentials, consistent with efficient hole injection from the carrier generation molecule chlorodiane blue in electrophotographic applications.

Concluding Remarks and Summary

The photooxidation of the hole transport molecule DEH gives rise to residual surface charges during light decay which cannot be photodischarged fast enough for electrophotographic applications. The "electrical fatigue" is attributed to a photochemically induced unimolecular rearrangement of DEH to an indazole derivative. By appropriate substitution of the DEH derivative, the photocyclization reaction and therefore the associated electrical fatigue is eliminated. Electrochemical and electrophotographic studies, in conjunction with the crystal structure of OMDEH, reveal that the hole-transport properties of DEH derivatives remain undisturbed by appropriate structural modifications, as long as the extended π system from the aniline amine nitrogen atom to the hydrazone phenyl group remain undisturbed.

(14) GAUSSIAN 88; Frisch, M. J.; Head-Gordon, M.; Schlegel, H. B.; Raghavachari, K.; Binkley, J. S.; Gonzalez, C.; Defrees, D. J.; Fox, D. J.; Whiteside, R. A.; Seeger, R.; Melius, C. F.; Baker, J.; Kahn, L. R.; Stewart, J. J. P.; Fluder, E. M.; Topiol, S.; Pople, J. A.; Gaussian, Inc.: Pittsburgh, PA, 1988.

(15) Jorgenson, W. L. *QCPE* **1980**, *12*, program 340.